Hyperspectral retinal imaging for micro- and nanoplastics detection: a conceptual and methodological framework

Tan Aik Kah

Eye Clinic, Normah Medical Specialist Centre, Kuching, Sarawak, Malaysia

ABSTRACT

This manuscript presents a conceptual and methodological framework rather than empirical results, outlining a pathway for applying hyperspectral retinal imaging (HSRI) to detect micro- and nanoplastics (MNPs). The retina, with its transparent optical media, layered architecture, and vascularization, offers an ideal biomedical model for adapting spectroscopic techniques that have been widely used in environmental and materials sciences. The framework consists of four staged phases: i) construction of a spectral library of common synthetic polymers; ii) phantom experiments replicating retinal optical properties spiked with defined MNPs; iii) *ex vivo* validation in ocular tissues with Raman and Fourier-transform infrared spectroscopy as chemical ground truth; and iv) pilot *in vivo* studies in small-animal models to assess HSRI sensitivity, specificity, and safety. Machine-learning classifiers and spectral unmixing algorithms are incorporated to separate polymer-specific signals from endogenous chromophores such as hemoglobin, melanin, and lipofuscin. While no experimental data are presented, the framework anticipates the establishment of polymer spectral libraries, demonstration of separable spectral signatures, and translational feasibility for detecting polymer deposits under safe irradiance conditions. If validated, HSRI could enable the retina to serve as a sentinel organ for systemic pollutant exposure, bridging ophthalmology, toxicology, and environmental health through spectroscopy.

GRAPHICAL ABSTRACT

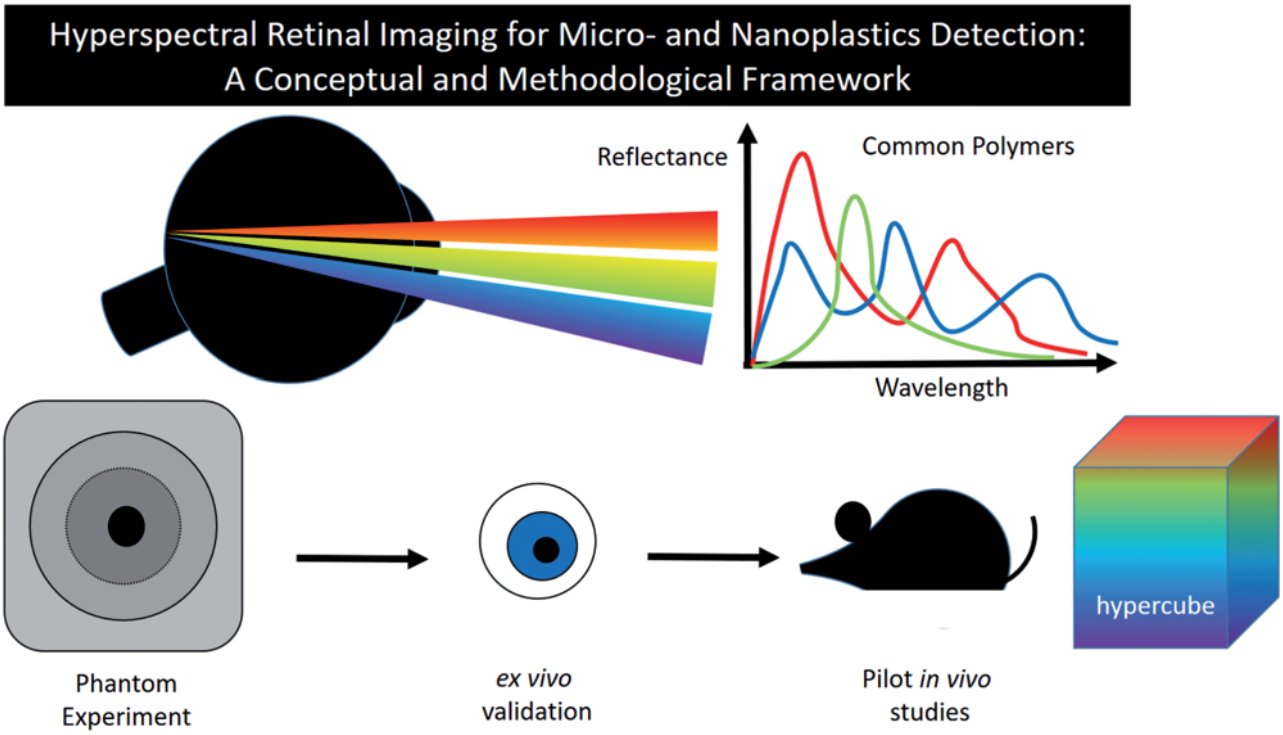

OPEN ACCESS

Introduction

Microplastics and nanoplastics (MNPs) have emerged as pervasive contaminants in air, water, food, and even human tissues. Growing evidence links these synthetic particles to oxidative stress, inflammation, and cellular toxicity across multiple organ systems, raising concerns about their potential contribution to chronic disease.[1-3] Recent studies have confirmed the presence of MNPs in human blood, placenta, lung, ocular fluids (vitreous and aqueous humor), and the retina, suggesting the eye may serve as both a target and sentinel of systemic plastic exposure.[4-7] A key rationale for selecting the eye -particularly the retina- as a biomarker of systemic exposure lies in its unique anatomical, physiological, and optical properties. The retina is the only neural and vascular tissue that can be imaged non-invasively at micron-scale resolution *in vivo*. Its dual circulation (retinal and choroidal) is directly influenced by systemic blood flow, making it sensitive to circulating xenobiotics, inflammatory mediators, and microvascular stress. Moreover, because the retina shares embryologic origins and barrier properties with the central nervous system (CNS), alterations in its optical or biochemical signatures may mirror neurovascular responses elsewhere in the body. This positions the retina as an accessible, translational proxy for systemic microvascular and toxicological processes. From a practical standpoint, ocular imaging is non-invasive, repeatable, and already widely used in clinical settings for systemic disease surveillance - offering a scalable platform for pollutant bio-monitoring. In this context, the retina represents an ideal site for an 'optical biopsy'.

Hyperspectral imaging integrates imaging and spectroscopy, capturing spatially resolved reflectance or absorbance spectra across hundreds of contiguous wavelength bands. By exploiting subtle differences in spectral fingerprints, hyperspectral imaging has become a powerful, non-destructive tool for polymer identification in environmental monitoring and for cellular imaging of nanomaterials.[8-9] Its ability to distinguish materials based on their intrinsic optical properties offers a unique opportunity to detect synthetic particles in biological tissues without exogenous labels. The retina offers a uniquely accessible neural and vascular tissue that reflects both local and systemic processes. Unlike most internal organs, it can be imaged directly and repeatedly at high resolution through the transparent ocular media. If MNPs accumulate within the neurosensory retina or retinal pigmented epithelium, hyperspectral imaging could serve as a noninvasive diagnostic window for systemic plastic exposure, analogous to how retinal imaging has been used as a biomarker for cardiovascular, neurodegenerative, and metabolic diseases.[10-11]

Hyperspectral imaging excels at identifying materials based on their unique spectral signatures.[12] Synthetic polymers such as polyethylene (PE), polypropylene (PP), polyethylene terephthalate (PET), polystyrene (PS), and polyvinyl chloride (PVC) exhibit distinct reflectance and absorption features, particularly in the visible–near infrared–short-wave infrared (VIS–NIR–SWIR) ranges, which differ markedly from those of endogenous retinal chromophores. This provides a basis for spectral differentiation between foreign particles and native tissue. The retina, being highly vascularized, metabolically active, and directly exposed to circulating and environmental influences, is also susceptible to foreign particle accumulation, as evidenced by reports of microplastics in ocular fluids and the retina.[4-7] Importantly, hyperspectral imaging has already been applied to detect exogenous materials -including nanoparticles, and amyloid aggregates- in other tissues, demonstrating its sensitivity to subtle compositional differences.[8,11] This study advances the hypothesis that MNPs in the human retina, exhibit distinct spectral signatures that can be differentiated from endogenous retinal chromophores (hemoglobin, melanin, lipofuscin) using hyperspectral retinal imaging (HSRI).

Methods

Feasibility and experimental pathway

To test this hypothesis, a stepwise validation strategy is proposed: i) compile a spectral library of common polymers (PE, PP, PET, PS, PVC) across the VIS-NIR-SWIR ranges to establish baseline fingerprints; ii) perform phantom experiments with tis-

Correspondence: Tan Aik Kah, Eye Clinic, Normah Medical Specialist Centre, Lot 937, Section 30 KTLD, Jalan Tun Abdul Rahman Yaakub, Petra Jaya, 93050 Kuching, Sarawak, Malaysia. E-mail: portwinestain@hotmail.com

Key words: microplastics; nanoplastics; hyperspectral retinal imaging.

Contributions: TAK, conceptualization, methodology, software, validation, data curation, writing – original draft preparation, writing – reviewing and editing, visualization, investigation, supervision. The author read and approved the final version of the manuscript and agreed to be accountable for all aspects of the work.

Conflict of interest: the author declares no competing interests, and confirms accuracy.

Declaration of generative artificial intelligent and artificial intelligent-assisted technologies in the writing process: in the preparation of this manuscript, the author utilized an artificial intelligence tool (ChatGPT, OpenAI GPT-5) to enhance efficiency, clarity, and precision. AI assistance was employed in several areas: generating preliminary drafts for sections such as the Methods and Discussion based on structured prompts, improving readability by rephrasing complex sentences and ensuring consistency in terminology. All AI-generated content was rigorously reviewed, edited, and validated by the author to ensure scientific accuracy and originality. The final manuscript reflects the author's intellectual input, clinical expertise, and critical analysis. No patient data or confidential information was entered into the AI system. AI was used solely as a productivity-enhancing tool to support, not a substitute for human reasoning and academic integrity.

Received: 14 October 2025.
Accepted: 3 December 2025.

Publisher's note: all claims expressed in this article are solely those of the authors and do not necessarily represent those of their affiliated organizations, or those of the publisher, the editors and the reviewers. Any product that may be evaluated in this article or claim that may be made by its manufacturer is not guaranteed or endorsed by the publisher.

©Copyright: the Author(s), 2025
Licensee PAGEPress, Italy
Advancements in Health Research 2025; 2:127
doi: 10.4081/ahr.2025.127

This article is distributed under the terms of the Creative Commons Attribution-NonCommercial International License (CC BY-NC 4.0) which permits any noncommercial use, distribution, and reproduction in any medium, provided the original author(s) and source are credited.

sue-mimicking scattering media spiked with MNPs of defined sizes to simulate retinal optics; iii) conduct *ex vivo* validation in ocular tissues or cadaveric eyes, using Raman or Fourier-transform infrared (FTIR) spectroscopy as ground truth; and iv) pilot *in vivo* studies in small animals to assess sensitivity, penetration depth, and specificity. This translational pipeline would define the technical limits of HSRI for detecting foreign particles and lay the foundation for non-invasive retinal monitoring as a biomarker of systemic plastic exposure (Figure 1).

Spectral library of common polymers

To establish baseline optical fingerprints, a spectral library of common synthetic polymers is proposed to be constructed. Five representative polymers (PE, PP, PET, PS, and PVC) will be obtained as commercial pellets, films, and size-fractionated particles (100 nm to 100 µm). Samples will be prepared by cryo-milling, sieving, or purchased as monodisperse beads. Reflectance spectra will be acquired across the VIS-NIR-SWIR ranges (400-1700 nm) using a benchtop integrating-sphere spectrometer (spectral resolution ≤10 nm in VIS-NIR, ≤20 nm in SWIR).[13] Imaging-based acquisitions will be performed with both snapshot and tunable hyperspectral cameras under calibrated broadband illumination. Dark current and white reference corrections (Spectralon) will be applied. Principal component analysis and cluster mapping will be used to visualize spectral separability between polymer types.

Importantly, the spectral library will account for environmental and biological aging effects. Alongside virgin polymer samples, artificially aged particles (ultraviolet exposure, mechanical weathering) and protein-corona coated samples incubated with vitreous humor or serum proteins should be characterized. This comprehensive approach acknowledges that *in vivo* MNPs undergo surface modifications that alter their optical properties. While protein coronas may dampen or shift certain spectral features in the visible range, the fundamental polymer backbone vibrations -particularly C-H overtones in the SWIR region- are expected to remain detectable beneath surface protein layers.[14-15]

Phantom experiments

To simulate retinal optics, multilayer tissue phantoms will be fabricated using agarose or silicone matrices incorporating scattering (1% intralipid) and absorption components (0.1 g/L hemoglobin analogs, synthetic melanin).[16-17] These materials will be selected for their well-characterized optical equivalence to biological tissues: agarose and silicone will provide controllable refractive indices and mechanical stability comparable to retinal and scleral layers, while diluted Intralipid (e.g., 0.2–1%) will approximate the reduced scattering coefficient of gray matter in neural tissue ($\mu'_s \approx 5\text{-}15\ cm^{-1}$ in the 500-900 nm range).[18-19] Hemoglobin analogs will reproduce hemoglobin's broad visible absorption peaks at 540-575 nm,[20] and synthetic melanin will mimic the near-infrared absorption tail of retinal pigmented epithelium and choroidal melanin. Together, these components will yield realistic optical scattering and absorption conditions for retinal-mimetic validation.

Phantoms will be spiked with known concentrations of polymer particles (10^2-10^6 particles/cm^2) at multiple depths: surface (vitreous-equivalent), mid-layer (retina-equivalent), and deep (retinal pigmented epithelium-equivalent). Detailed phantom recipe available in *Appendix A*. Hyperspectral image cubes will be acquired under standardized illumination with spectral sampling of 5-10 nm in VIS-NIR and 10-20 nm in SWIR. Ground-truth particle localization will be confirmed by confocal

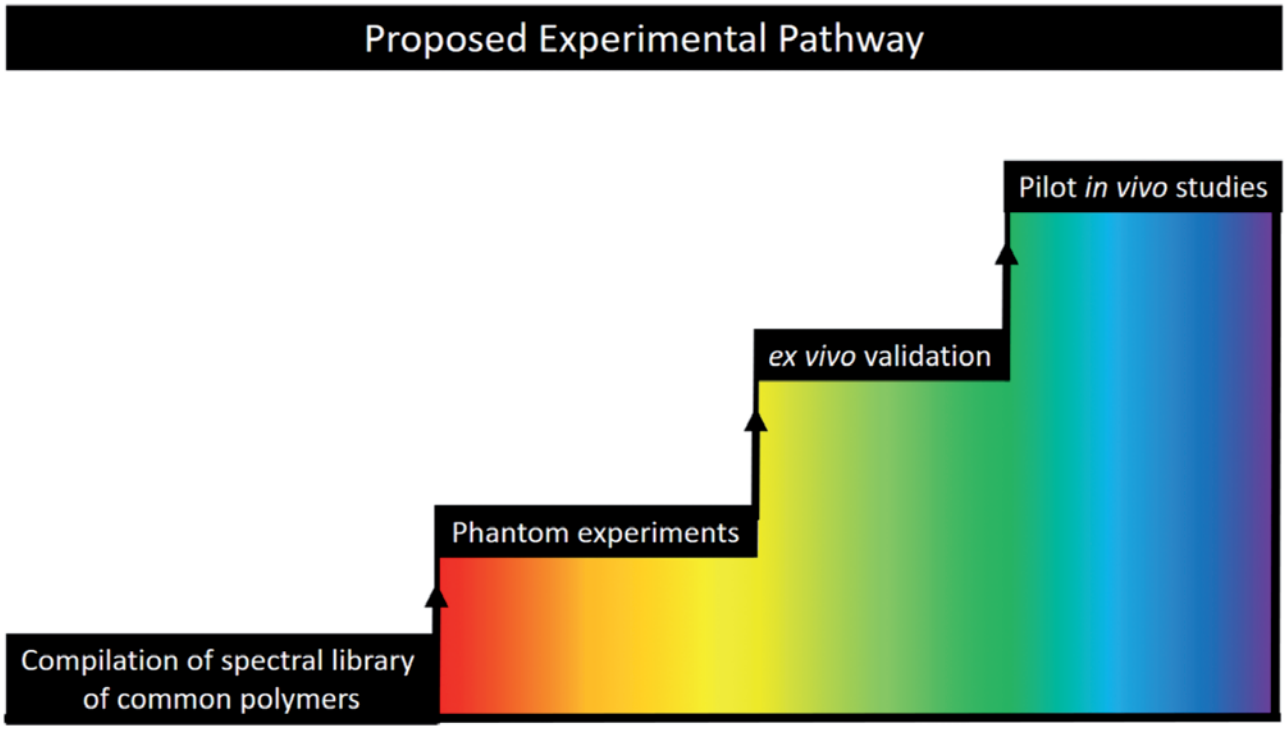

Figure 1. Proposed experimental pathway.

OPEN ACCESS

microscopy or enhanced dark-field microscopy. Detection thresholds will be defined as the smallest particle size and lowest surface density consistently identified across replicates (n ≥5 per condition).

While a variety of ocular phantoms exist for structural modalities such as OCT and fundus imaging, HSRI–specific phantoms remain limited. Previous HSRI efforts have emphasized either anatomical realism or oxygenation mapping using 3D-printed or blood-based constructs.[21,22] The present phantom is designed to complement these by providing a layered, compositionally tunable model that reproduces the spectral, scattering, and absorbing features of retinal tissue without the need for biological material. Through controlled incorporation of hemoglobin, melanin (or India ink), and Intralipid, the design will enable reproducible spectral calibration and validation of HSRI systems, as well as quantitative embedding of particulate inclusions at defined densities - capabilities not addressed in prior phantoms (Table 1). This modular, reproducible structure is expected to bridge the gap between computational modeling and biological experiments in HSRI validation.

In addition to static phantoms for establishing fundamental detection thresholds, dynamic phantom experiments will be performed to validate motion compensation algorithms essential for clinical application. A motorized translation stage (e.g., Physik Instrumente M-126.DG1 or equivalent) will be integrated to simulate physiological eye movements including microsaccades (0.1-0.3° amplitude, 30-100 Hz frequency), physiological tremor (30–100 Hz, <0.1° amplitude), and slow drift (0.1-0.5°/s velocity). Motion parameters will be based on established ocular physiology literature, including microsaccade dynamics,[23] physiological tremor characteristics,[24] and ocular drift velocity studies.[25] Hyperspectral image cubes will be acquired during simulated motion to test the robustness of motion compensation algorithms described in the section *Data analysis*, spectral unmixing accuracy under realistic motion conditions, and polymer detection sensitivity with pixel misregistration. Performance metrics will include motion-induced spectral distortion, unmixing error rates, and detection threshold degradation compared to static conditions.

Imaging hardware and protocol

Two HSRI configurations will be evaluated: i) a snapshot system employing Bayer filter mosaic or Fabry–Pérot array sensors, and ii) a tunable liquid-crystal filter system.[26-27] For the tunable liquid-crystal filter system, motion robustness will be explicitly evaluated using the dynamic phantom platform. Given that tunable systems acquire spectral bands sequentially over time (typically 1-5 s for full spectral cubes), motion compensation is critical for maintaining pixel-to-pixel spectral alignment, a prerequisite for reliable micron-scale particle detection. The snapshot HSRI system will serve as a motion-resistant benchmark for comparison.

Imaging parameters will include a spatial resolution equivalent to ~100-200 µm per retinal pixel and a field of view of 30-50°.[28] All systems will be radiometrically calibrated, with dark/white corrections and flat-field normalization applied. Signal-to-noise ratio (SNR) targets will be set at >40 dB per spectral band. Retinal irradiance levels will be maintained within American National Standards Institute and International Organization for Standardization safety standards.[29]

Based on established biomedical hyperspectral imaging performance and the SNR calculations above, the expected detection threshold for MNPs in the retina is anticipated to fall within the micron-to-submicron range for particle size and at or above 10^{-4}-10^{-3} volume fraction for concentration.[7,30] While the *in vivo* spatial resolution (~100 µm per pixel) will preclude visualization of individual particles, my quantitative modeling indicates that localized aggregates of approximately 80-100 microplastic particles or several thousand nanoplastics per pixel volume can produce detectable spectral anomalies ($\Delta R \geq 1\%$) through their collective scattering and absorption effects (*Appendix E*).[30] These particle densities are biologically plausible given reported MNP accumulation in other tissues and represent concentrations that could occur in retinal structures acting as accumulation sites.[31-33]

Although individual nanoplastics will be well below the optical resolution limit, their detection may still be feasible through indirect spectral manifestations. Nanoplastics can alter local refractive indices, induce subtle changes in scattering coefficients, or form aggregates that shift overall spectral reflectance or absorption profiles within a pixel cluster. Moreover, secondary biological responses, such as microglial activation or pigment granule redistribution, could amplify these spectral perturbations, allowing indirect inference of nanoplastic presence through pattern recognition and spectral unmixing analysis. These mechanisms will be explored conceptually in the subsequent feasibility and validation phases.

Ground-truth chemical validation

Polymer identification will be confirmed by chemical and morphological analyses. Raman spectroscopy and Fourier-transform infrared (FTIR) microscopy will be employed for spatially resolved polymer typing.[34] Pyrolysis-gas chromatography-mass spectrometry (Py-GC-MS) will be used for bulk confirmation of polymer type and quantity.[35] For phantom and *ex vivo* tissues, regions of interest identified by HSRI will be microdissected and

Table 1. Comparison of existing ocular phantoms relevant to hyperspectral retinal imaging (HSRI).

Study/phantom	Key features	Main limitation	How present work improves/complements
Ghassemi *et al.*[21]	3D-printed vascular channels with blood; emphasis on anatomical realism and perfusion	Limited spectral tunability; requires biological blood	Provides non-biological, compositionally tunable layers; spectral properties reproducible
Bryarly *et al.*[22]	3D-printed mouse retina phantom with deoxygenated blood for oxygenation mapping	Focused on oxygenation studies; not modular or particulate-compatible	Enables quantitative embedding of particles and spectral calibration without blood
Current work	Layered agarose/gelatin phantom with controlled hemoglobin, melanin (or ink), and Intralipid	Limited anatomical realism; short-term stability (1-2 weeks at 4°C)	Bridges spectral realism, reproducibility, and modular validation of HSRI systems

analyzed with Raman/FTIR mapping. Scanning and transmission electron microscopy will be applied for morphological confirmation and size distribution.[36]

Ex vivo and *in vivo* pilot studies

All human tissue use will adhere to the Declaration of Helsinki and institutional guidelines, and animal protocols will be approved by Institutional Animal Care and Use Committee-approved. *Ex vivo* studies will be conducted using cadaveric human eyes (with institutional approval) and freshly enucleated animal eyes (pig and rabbit). Tissues will be spiked with polymer suspensions either within the vitreous or directly onto the retinal surface prior to HSRI. Ground-truth chemical analyses will be performed as described above.

For *in vivo* studies, small animals (rodents and rabbits) will be used. Polymer suspensions will be administered via intravitreal or systemic routes at ethically approved doses. Longitudinal HSRI imaging will be performed at baseline, acute (24 h), and subacute (72 h) timepoints, followed by *ex vivo* tissue harvesting and chemical validation.

Sample size selection will be informed by prospective statistical power calculations (*Appendix B*). These analyses are expected to indicate that large detection effects (e.g., 50–60% spectral anomaly rate *vs* ≤5% false positives) can be detected with 10-15 samples per group, while medium continuous effect sizes (Cohen's d ≈0.5) will require ~60 per group. Accordingly, pilot designs (5-10 phantom replicates, 20-30 *ex vivo* tissues, 8-15 animals) will be chosen to balance feasibility and statistical power (1-β=0.8, α=0.05). Classifier performance will be evaluated using k-fold cross-validation, and group comparisons will employ two-sided tests, with $p<0.05$ considered significant.

Data analysis and classification

Preprocessing will include dark/white correction, motion compensation (for tunable systems), spectral smoothing (Savitzky-Golay), and registration to high-resolution fundus images. Motion compensation will employ a multi-stage approach: i) feature-based registration using retinal vasculature patterns or phantom fiducials; ii) optical flow estimation for inter-frame motion correction; and iii) robust spectral unmixing algorithms (e.g., partially constrained non-negative matrix factorization) that are less sensitive to residual misregistration. Performance will be quantified using motion-corrupted data from dynamic phantom experiments. Spectral unmixing will be performed using linear and non-linear algorithms, including non-negative matrix factorization and spectral angle mapping. Machine learning classifiers (support vector machines, random forests) will be trained on spectral library and phantom data. Deep learning methods (2D/3D convolutional neural networks) will be explored for spectral-spatial feature learning. Performance metrics will include sensitivity, specificity, precision, recall, F1-score, and area under the receiver operating curve. Detection limits will be reported as minimum particle density (particles/mm^2) with acceptable sensitivity and specificity. Polymer classification performance will be summarized using confusion matrices.

Controls and statistical analysis

Negative controls will include unspiked phantoms and tissues, while positive controls will include spiked samples with known polymer types. Biological confounders (hemoglobin, melanin, lipofuscin) will be incorporated into phantom experiments to test specificity. All conditions will be performed in replicates (n ≥5 for phantom studies, ≥10 *ex vivo* samples per polymer). For animal pilots, 6-10 animals per group will be used to estimate variance. Data will be analyzed using k-fold cross-validation for classifier performance, and statistical comparisons will be made using two-sided tests with $p<0.05$ considered significant.

Computational proof-of-concept validation

To address the fundamental question of spectral separability between synthetic polymers and biological chromophores, I performed a computational simulation using mathematically generated spectral profiles (Appendices C and D). Synthetic reflectance spectra were created for hemoglobin (characteristic dual absorption peaks at 540 nm and 575 nm),[37] melanin (broadband wavelength-dependent absorption),[38] polyethylene (distinct C-H overtone features at 930 nm, 970 nm, 1210 nm, and 1730 nm),[39] and polystyrene (characteristic absorptions at 1180 nm and 1600-1660 nm double-feature).[40] These profiles were designed to capture the key optical properties of each material based on established spectroscopic literature (Figure 2).

Two simplified synthetic mixtures were generated to model trace polymer presence within a biological background (Bio). First, a composite retinal tissue spectrum was created by combining hemoglobin (70%) and melanin (30%). Polyethylene (2%) and polystyrene (3%) were then separately introduced into this background to produce Bio + PE and Bio + PS mixtures, respectively. These low polymer fractions (2-3%) were selected to illustrate conceptual spectral mixing rather than to represent physiological concentrations. Ratio-based normalization was applied to evaluate whether small polymer-associated spectral perturbations could, in principle, be distinguished from the dominant biological signal under idealized, noise-limited conditions.[41-42]

Correlation analysis of the normalized spectra provided a preliminary indication of theoretical separability under idealized conditions. The polyethylene ratio signal showed a moderate correlation with the pure polyethylene spectrum (r=0.63), while the polystyrene ratio signal demonstrated a similar correlation with the pure polystyrene spectrum (r=0.65). These values suggest that small polymer-associated spectral perturbations may, in principle, be recoverable from a dominant biological background when evaluated mathematically.

Specificity remained acceptable, with low cross-correlations between the polyethylene ratio signal and the polystyrene spectrum (r=0.11), and between the polystyrene ratio signal and the polyethylene spectrum (r=0.21), indicating limited risk of spectral misattribution in this simplified setting. However, when simulated measurement noise was introduced, the polyethylene detection correlation decreased to r=0.29, reflecting the substantial challenge of extracting weak polymer signals under realistic imaging conditions (Table 2).

These results demonstrate that: i) spectral separability is theoretically feasible; ii) biological dominance presents a measurable but surmountable challenge; and iii) advanced analytical methods are required for robust polymer detection - precisely validating the need for the machine learning and spectral unmixing approaches proposed in this framework.

These simulations represent idealized spectral profiles. In biological environments, protein corona formation and surface modifications may attenuate or shift certain spectral features, particularly in the visible range.[32-33] However, the fundamental

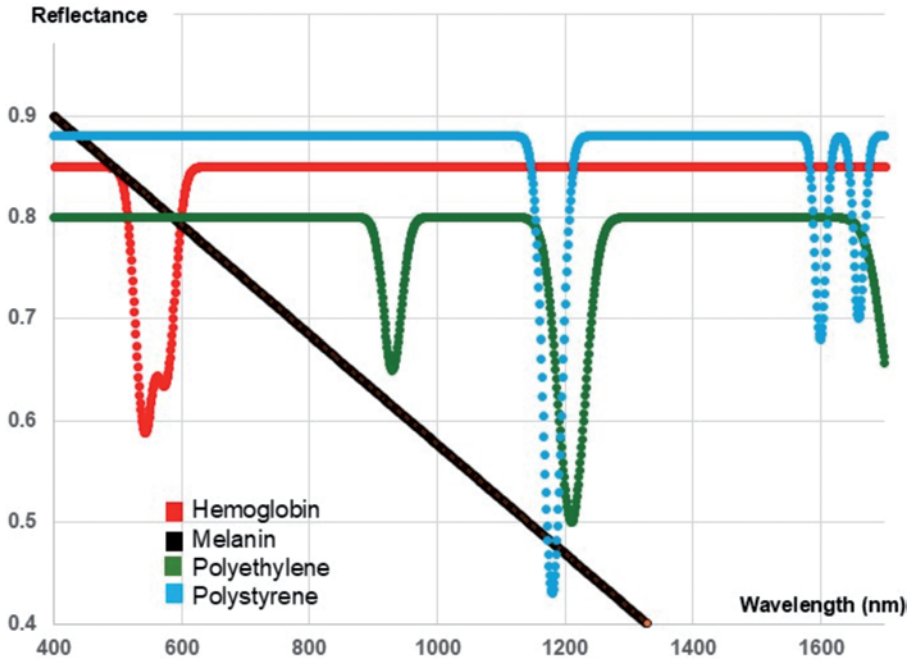

Figure 2. Computational spectral profiles for retinal chromophores and synthetic polymers. Synthetic reflectance spectra were generated to model the characteristic optical properties of hemoglobin (dual absorption peaks at 540 nm and 575 nm), melanin (broadband wavelength-dependent absorption), polyethylene (C-H overtone features at 930 nm, 970 nm, 1210 nm, and 1730 nm), and polystyrene (characteristic absorptions at 1180 nm and 1600-1660 nm double-feature). These profiles provide the theoretical basis for spectral separability in hyperspectral retinal imaging.

polymer backbone vibrations simulated here, especially in the SWIR region (>1000 nm), are expected to be more resilient to such surface alterations.[39-40]

Signal-to-noise ratio estimation for MNPs detection

To quantitatively assess the feasibility of detecting sub-resolution MNPs, I performed SNR calculations based on established light scattering theory. For a 100 µm pixel, the minimum detectable signal change (ΔR) can be estimated as:

$$\Delta R_{min} = \frac{1}{SNR_{target}} \quad \text{(Eq. 1)}$$

Assuming a conservative SNR of 40 dB (100:1) as previously specified, ≈ 0.01 (1% reflectance change).

The spectral perturbation caused by MNP aggregates can be modeled using Mie scattering theory. For polystyrene spheres (n=1.59) in aqueous medium (n=1.33) at 500 nm wavelength, the scattering cross-section for a 1 µm particle is approximately 1.2 µm^2. Within a 100 µm × 100 µm × 100 µm retinal volume (10^{-6} cm^3), the number of particles required to produce 1% reflectance change is:

$$N_{particle} = \frac{\Delta R \cdot A_{pixel}}{\sigma_{sca}} \approx (0.01 \times 10^4\ \mu m^2) / 1.2\ \mu m^2 \approx 83\ \text{particles} \quad \text{(Eq. 2)}$$

This corresponds to a volume fraction of ~4.3×10^{-5}, or approximately 0.0043%, which falls within the 10^{-4}–10^{-3} range proposed in the previous paragraph. For nanoplastics (100 nm), the required particle count increases to ~8,300 due to reduced scattering efficiency, but remains physiologically plausible given reported MNP accumulation densities in human tissues, including recent evidence of microplastic deposition in the retina and nanoplastic accumulation in the brain and systemic circulation.[7,31-33]

These calculations demonstrate that MNP detection at HSRI resolution limits is mathematically feasible through collective scattering effects, provided sufficient local accumulation occurs (*Appendix E*).

Table 2. Results of computational analysis.

Analysis	Correlation coefficient	Interpretation
PE ratio correlation	0.63	Moderate detection
PS ratio correlation	0.65	Moderate detection
Specificity		
(PE ratio *vs* PS)	0.11	Low, indicating good specificity
(PS ratio *vs* PE)	0.21	Low, indicating good specificity
Noisy PE ratio detection	0.29	Weak but detectable above noise

Proposed validation framework

As this study proposes a methodological framework rather than presenting experimental measurements, I first provide preliminary computational evidence to examine whether polymer-associated spectral perturbations could, in principle, be distinguished from biological backgrounds. The results suggest that spectral features can potentially be mathematically separated, providing foundational support for the proposed experimental framework. Subsequent validation pathway will empirically test this principle through: i) demonstration of separable polymer spectral signatures, particularly in regions corresponding to C-H overtone and combination bands distinct from endogenous retinal chromophores; ii) validation of HSRI against chemical ground-truth methods; and iii) feasibility testing under safe ocular irradiance conditions.

To operationalize this workflow, the anticipated validation pathway is structured as a stepwise progression to establish both technical feasibility and translational relevance. The validation pathway will also incorporate dynamic testing to ensure clinical relevance: static phantoms establish fundamental sensitivity limits, dynamic phantoms validate motion robustness, *ex vivo* tissues test biological complexity, and *in vivo* studies confirm clinical feasibility.

Human-scale multilayer phantoms will first be used in both static and dynamic configurations to systematically evaluate polymer detectability across depth, spectral range, and concentration, establishing quantitative thresholds for sensitivity and specificity. Findings from these phantom studies will guide *ex vivo* validation in cadaveric or freshly enucleated eyes, enabling direct comparison of HSRI spectral anomalies with chemical ground-truth methods such as Raman or FTIR spectroscopy to verify polymer localization. Building on these results, pilot *in vivo* studies in small animals will assess non-invasive detection, temporal reproducibility, and robustness against biological confounders including hemoglobin, melanin, and lipofuscin (see the Graphical Abstract). Success in each phase will be determined by reliable separation of polymer spectral signatures from endogenous chromophores, reproducible detection across replicates, and quantitative agreement with chemical validation. By integrating phantom-based calibration with *ex vivo* and *in vivo* studies, this structured approach provides a clear roadmap for translating HSRI toward potential clinical monitoring of systemic pollutant exposure.

Discussions

In this discussion, I contextualize the proposed methodological framework by outlining the anticipated validation pathway, comparing the phantom design to existing ocular models, and specifying expected performance targets for HSRI. This framing emphasizes the manuscript's focus on reproducibility, translational relevance, and practical utility for preclinical and eventual clinical applications.

Feasibility and strengths

HSRI offers several inherent advantages for detecting MNPs within retinal tissue. Unlike biological chromophores, synthetic polymers often exhibit distinct and relatively simple spectral fingerprints, particularly in the VIS-NIR and SWIR domains. These differences arise from their unique chemical composition, polymer backbone structure, and the presence of additives such as dyes and stabilizers, which further enhance spectral separability.[43] In contrast to the biochemical complexity of living tissues, plastics generally produce sharper and more stable optical signatures, simplifying their classification once appropriate spectral libraries are established.

Furthermore, HSRI leverages the exceptional optical accessibility of the retina. The eye is uniquely transparent, enabling direct and repeatable visualization of neural and vascular tissues without invasive procedures. This makes the retina an ideal 'optical biopsy' site for systemic exposure monitoring. Retinal imaging has already demonstrated its sensitivity as a biomarker platform for diverse systemic diseases, including diabetes, neurodegeneration, and cardiovascular disease, establishing a translational precedent for pollutant exposure.[10,11] If MNPs accumulate in the vitreous, inner retina, or retinal pigmented epithelium, their presence should be detectable as spectral anomalies, particularly when aided by advanced spectral unmixing algorithms and machine-learning classifiers trained on reference datasets.

My computational simulations suggest the theoretical possibility of distinguishing plastic signals from biological noise. This finding strengthens the need for the sophisticated unmixing algorithms proposed in this framework and provides mathematical proof that polymer-specific signatures are theoretically separable from biological chromophores when appropriate analytical techniques are employed.

Challenges and limitations

Despite these opportunities, significant challenges must be overcome before HSRI can be applied as a reliable diagnostic for environmental pollutant exposure. The foremost limitation is particle size. Current HSRI systems, such as the one described in this study, achieve spatial resolutions of approximately 100–200 µm per pixel, enabling detection of larger microplastics but placing smaller micron-scale and nanoscale particles below the optical resolution threshold.[28] Unless nanoplastics form aggregates or induce secondary optical effects such as scattering or local inflammatory changes, they may escape *in vivo* detection. While my SNR calculations demonstrate the theoretical feasibility of detecting MNP aggregates, practical detection requires sufficient local particle density. In scenarios where MNPs are sparsely distributed without forming dense aggregates, the spectral signal may fall below detection thresholds. This limitation particularly affects nanoplastics, which require higher particle counts due to their reduced scattering efficiency. Future technological improvements in SNR and spatial resolution will be necessary to detect lower concentration distributions.

The tunable-filter HSRI configuration faces particular challenges from ocular motion during sequential spectral acquisition. Even sub-pixel displacements between spectral band acquisitions can degrade unmixing performance for small targets like microplastics. While the current proposed dynamic phantom validation and advanced motion compensation algorithms address this limitation, residual motion artifacts may ultimately favor snapshot HSRI approaches for *in vivo* applications requiring high spatial precision.

A second limitation is spectral overlap.[44] While synthetic polymers exhibit characteristic absorption features, these often coincide with endogenous retinal chromophores, including hemoglobin, melanin, lipids, and lipofuscin. The retina's layered, vascularized, and pigment-rich architecture further complicates analysis, increasing the likelihood of false positives. Resolving such ambiguities will require high spectral resolution systems, ro-

bust spectral libraries, and advanced computational approaches for spectral unmixing.

A critical consideration for clinical translation is the modification of MNP spectral properties in biological environments. Upon entering ocular fluids, plastics rapidly acquire protein coronas that can alter surface reflectance characteristics, particularly in the visible range. Additionally, environmental aging prior to biological exposure further modifies spectral signatures through photo-oxidation and surface weathering. However, the fundamental vibrational modes of polymer backbones -especially C-H stretching overtones in the 1600–1800 nm SWIR range- are less susceptible to surface modifications and may provide more robust detection targets.[39-40] The spectral library approach explicitly addresses this by including both virgin and biologically exposed particles to establish detection boundaries and identify the most stable spectral features for reliable *in vivo* identification.

In addition to spectral overlap, several biological and optical factors can confound HSRI interpretation. Inter-individual variability in ocular pigmentation, particularly melanin concentration within the retinal pigmented epithelium and choroid, alters baseline reflectance profiles and can mimic or obscure polymer-associated spectral features. Media opacities such as cataract or vitreous haze reduce signal intensity and spectral fidelity, while retinal diseases (especially those causing hemorrhage, exudation, or fibrosis) introduce secondary reflectance changes unrelated to environmental particles. Future studies should incorporate standardized correction factors or reference normalization methods to mitigate these physiological confounders.

Finally, issues of sensitivity, depth penetration, and validation remain unresolved. HSRI reflectance signals primarily originate from superficial retinal layers, making particles in the vitreous or inner retina more accessible than those within the retinal pigmented epithelium or deeper layers. Establishing reliable *ex vivo* and *in vivo* validation models will therefore be essential. At present, direct correlations between retinal spectral anomalies and systemic plastic exposure remain sparse. Clinical translation will require rigorous cross-validation against histopathological and biochemical evidence of polymer accumulation, complemented by chemical ground-truth methods such as Raman or FTIR spectroscopy, to define detection thresholds, estimate false positive rates, and establish biological specificity.

Standardization and reproducibility

Beyond optical and biological limitations, a critical barrier to clinical translation lies in the lack of standardization across hyperspectral imaging platforms. Differences in illumination geometry, spectral calibration, detector sensitivity, and preprocessing pipelines can yield substantial variability in reflectance spectra, even for identical biological samples. Currently, no universally accepted reference phantoms or calibration standards exist for retinal HSRI, complicating cross-device comparability and meta-analysis.

Reproducibility is further challenged by the diversity of spectral unmixing algorithms and machine learning pipelines, many of which are non-transparent or dataset-specific. Small variations in preprocessing, such as baseline correction, smoothing, or normalization, can alter classification outcomes. To ensure reproducibility and regulatory readiness, future studies should adopt open, benchmarked workflows and publish raw hyperspectral datasets whenever possible. Inter-laboratory validation using standardized calibration targets and reporting guidelines, analogous to the Minimum information about a microarray experiment (MIAME) standard in genomics or the QUAREP-LiMi initiative in microscopy, would substantially strengthen methodological rigor in environmental ophthalmic imaging.[45-46]

Comparison with existing MNP detection techniques

Existing analytical methods for detecting MNPs, including Raman and FTIR microscopy, and Py–GC–MS, provide well-established chemical identification standards. However, their methodological characteristics differ markedly from those of HSRI, particularly regarding applicability to *in vivo*, noninvasive, and clinical contexts.

Raman and FTIR microscopy achieve exceptional *chemical specificity* (submicron resolution, unique vibrational fingerprints) and *sensitivity* to particle composition, but they require *physical sampling* of tissues, often involving fixation, sectioning, and labeling.[34] Their scanning-based nature limits *throughput*, as mapping even a few square millimeters may require hours. These constraints restrict their clinical scalability to *ex vivo* or biopsy-based analyses.

Py-GC-MS, in turn, provides high *analytical sensitivity* and *quantitative polymer identification*, detecting nanogram-scale plastic loads with high precision. Yet it is *fully destructive* and lacks spatial or morphological information.[35] Consequently, it is suitable only for bulk chemical analysis of extracted samples.

By contrast, **HSRI** is *non-invasive, label-free, and real-time*, enabling wide-field spectral mapping of the intact retina without sample removal. Although its *spectral specificity* is lower due to broader bandwidths and mixed optical scattering effects, HSRI offers substantial advantages in *throughput* and *clinical scalability*. It can image millions of retinal pixels in seconds under safe irradiance, allowing longitudinal, *in vivo* monitoring of MNP accumulation or clearance, capabilities unattainable by conventional analytical techniques. HSRI is thus best viewed as a *screening and surveillance platform* complementary to Raman/FTIR and Py–GC–MS. Together, they form a translational pipeline: HSRI for *non-invasive detection and localization*, Raman/FTIR for *chemical ground truth validation*, and Py–GC–MS for *quantitative compositional profiling* (Table 3).

In summary, HSRI does not compete directly with Raman, FTIR, or Py–GC–MS in analytical resolution, but complements them as a *translational, in vivo imaging modality*. Its value lies in enabling *population-scale, repeatable screening* for environmental pollutant exposure using the eye as an accessible optical window, thereby bridging clinical ophthalmology and environmental toxicology.

Implications and future directions

Despite these hurdles, the scientific rationale remains compelling. Precedents exist for hyperspectral imaging in other organs.[47-50] Together, these lines of evidence suggest that HSRI could feasibly serve as a sensitive probe for pollutant burden *in vivo*, provided technical refinements are achieved.

The ability to detect MNPs in the retina carries profound implications for environmental health surveillance. Unlike blood or urine assays, retinal imaging offers a non-invasive, repeatable, and longitudinally tractable method to assess pollutant exposure in living individuals. Such a tool could enable population-scale monitoring of environmental toxicants, serving as a biomarker platform that is dynamic, cost-effective, and compatible with routine ophthalmic examination.

Table 3. Comparison of HSRI and existing MNP detection techniques.

Feature	HSRI	Raman / FTIR microscopy	Py-GC-MS
Detection principle	Optical reflectance/absorbance spectra (VIS-NIR-SWIR)	Molecular vibrational spectroscopy	Thermal decomposition + chromatographic/mass spectral analysis
Sensitivity (detection limit)	Moderate (≥few µm particles or aggregates)	High (≤1 µm for Raman; ~10 µm for FTIR)	Very high (ng-µg polymer quantities)
Specificity (chemical discrimination)	Moderate (distinct but overlapping spectral bands)	Very high (molecular-level fingerprint)	Very high (polymer-type resolved)
Spatial resolution	~100-200 µm/pixel (optical limit)	~0.5-10 µm (depends on setup)	None (bulk measurement only)
Sample type	*In vivo*, intact tissue	*Ex vivo*, thin sections or filters	Extracted/destructive samples
Throughput	High (seconds per full image cube)	Low (minutes-hours per mm^2)	Moderate (minutes per sample)
Quantitative capability	Semi-quantitative (relative signal intensity)	Semi-quantitative (particle count, ID)	Fully quantitative (polymer mass fraction)
Clinical scalability	Excellent (noninvasive, repeatable, real-time)	Poor (requires biopsy or tissue extraction)	None (destructive, lab-based)
Operational environment	Ophthalmic imaging suite	Analytical spectroscopy lab	Analytical chemistry lab
Ideal application	Noninvasive screening and monitoring of pollutant burden	Chemical validation and mapping	Bulk compositional analysis and confirmation

Beyond exposure detection, HSRI may facilitate the early identification of pollutant-related retinal and systemic diseases. MNPs have been implicated in oxidative stress, vascular dysfunction, and neuroinflammation, all of which intersect with the pathophysiology of diabetic retinopathy, glaucoma, and age-related macular degeneration.[1] Detecting pollutant-induced changes at a subclinical stage could open new avenues for preventive intervention, ultimately reducing disease burden through early risk stratification. This aligns with the global push toward predictive and preventive healthcare paradigms.

Finally, the extension of HSRI into toxicology and public health represents a paradigm shift. While traditional methods of assessing plastic exposure rely on *ex vivo* spectroscopy or destructive chemical assays, retinal HSRI provides an opportunity to capture pollutant accumulation non-invasively and in real time. This could catalyze trans-disciplinary research bridging ophthalmology, toxicology, environmental health, and policy, thereby positioning the retina as a sentinel tissue for systemic pollutant burden.[6] By merging environmental medicine with advanced optical imaging, this approach holds promise not only for expanding HSRI's clinical utility but also for informing global strategies to mitigate the health impacts of plastic pollution.

These implications set the stage for future directions. Integration of HSRI with artificial intelligence–driven spectral analysis could enable automated identification of polymer-specific signatures in complex retinal datasets. Supervised and unsupervised machine learning classifiers, trained on comprehensive spectral libraries of common plastics, have the potential to markedly improve specificity and sensitivity by separating subtle plastic signals from the spectral background of native tissue.

In defining its translational trajectory, HSRI could serve three complementary purposes: i) a population-level *screening tool* for systemic pollutant exposure, where moderate sensitivity but high throughput is prioritized; ii) a *diagnostic adjunct* for confirming exposure in individuals with suspected pollutant-related disease, requiring higher specificity and standardized calibration; and iii) a *quantitative research instrument* for estimating relative exposure burden in epidemiological or toxicological studies. Each application imposes distinct performance thresholds and validation requirements, which will guide future optimization and regulatory evaluation.

In parallel, advances in pansharpening and super-resolution algorithms may address the current spatial resolution limitations of HSRI, enabling the detection of smaller microplastics and possibly nanoscale aggregates.[51] Furthermore, multimodal imaging platforms- for example, combining HSRI with optical coherence tomography, fluorescence imaging, or adaptive optics- could add structural, functional, and molecular context, thereby strengthening the reliability of pollutant detection and localization within the retina.

To ensure reproducibility and facilitate cross-platform comparability, future work should prioritize the development of an open-access spectral database of common polymers measured within biological matrices, including ocular tissues. Such a repository would allow calibration of hyperspectral systems across laboratories, support algorithm benchmarking, and enable transparent validation of polymer-specific signatures under controlled biological conditions. By providing standardized reference spectra, this initiative would accelerate methodological convergence and strengthen the translational pathway from research prototypes to clinical and regulatory applications. Framed in public health terms, HSRI could serve as a regulatory-relevant, population surveillance tool analogous to bio-monitoring frameworks used for heavy metals or air pollutants, providing real-time, noninvasive exposure assessment that informs policy and preventive interventions.

Conclusions

Together, these advances point toward a future in which HSRI could become a clinically viable tool for environmental toxicology and public health. The convergence of optical imaging, computational analytics, and systems-level biology may ultimately allow pollutant exposure to be monitored at the level of the individual patient, offering unprecedented opportunities for early detection, preventive intervention, and population-scale risk assessment.

References

1. Kadac-Czapska K, Ośko J, Knez E, Grembecka M. Microplastics and oxidative stress-current problems and prospects. Antioxidants 2024;13:579.
2. Bora SS, Gogoi R, Sharma MR, et al. Microplastics and human health: unveiling the gut microbiome disruption and chronic disease risks. Front Cell Infect Microbiol 2024;14: 1492759.
3. Gałęziewska J, Gromek P, Kruczkowska W, et al. Evaluating the relationship between microplastics and nanoplastics contamination and diverse cancer types development. Environ Pollut 2025;385:127052.
4. Zhang K, Yu L, Qu L, et al. Identifying and analyzing the microplastics in human aqueous humor by pyrolysis-gas chromatography/mass spectrometry. iScience 2025;28:112078.
5. Zhong Y, Yang Y, Zhang L, et al. Revealing new insights: two-center evidence of microplastics in human vitreous humor and their implications for ocular health. Sci Total Environ 2024; 921:171109.
6. Kah TA. A Bayesian approach to investigating presumed retinal micro(nano)plastics. Biosystems 2025;253:105502.
7. Zhang M, Liu S, Wang Y, et al. Environmental science & technology letters. Environ Sci Technol Lett 2025;12:1327–33.
8. Faltynkova A, Wagner M. Developing and testing a workflow to identify microplastics using near infrared hyperspectral imaging. Chemosphere 2023;336:139186.
9. Zhang HJ, Zhou HR, Pan W, et al. Accumulation of nanoplastics in human cells as visualized and quantified by hyperspectral imaging with enhanced dark-field microscopy. Environ Int 2023;179:108134.
10. Saeed A, Hadoux X, van Wijngaarden P. Hyperspectral retinal imaging biomarkers of ocular and systemic diseases. Eye 2025;39:667-72.
11. Ng YB, Sung SF, Nguyen HT, et al. Amyloid beta biomarker for dementia detection by hyperspectral ophthalmoscope images. Aging 2024;16:13648-61.
12. Karim S, Qadir A, Farooq U, et al. Hyperspectral imaging: a review and trends towards medical imaging. Curr Med Imaging 2022;19:417-27.
13. Zhang X, Qiu J, Li X, et al. Complex refractive indices measurements of polymers in visible and near-infrared bands. Appl Opt 2020;59:2337-44.
14. Lee H. Recent advances in simulation studies on the protein corona. Pharmaceutics 2024;16:1419.
15. Bashiri G, Padilla MS, Swingle KL, et al. Nanoparticle protein corona: from structure and function to therapeutic targeting. Lab Chip 2023;23:1432-66.
16. Ntombela L, Adeleye B, Chetty N. Low-cost fabrication of optical tissue phantoms for use in biomedical imaging. Heliyon 2020;6:e03602.
17. Kulmaganbetov M. Advancements in retinal tissue-mimicking optical coherence tomography phantoms: materials, properties, and applications. BioChem 2025;5:6.
18. Flock ST, Jacques SL, Wilson BC, et al. Optical properties of Intralipid: a phantom medium for light propagation studies. Lasers Surg Med 1992;12:510-9.
19. Ali JH, Bogdanovich S. Optical property measurements in normal human brain tissues: exploring discrepancies in the visible-NIR region. Biomed J Sci Tech Res 2023;51:008077.
20. Nadithe V, Bae YH. Synthesis and characterization of hemoglobin conjugates with antioxidant enzymes via poly(ethylene glycol) cross-linker (Hb-SOD-CAT) for protection from free radical stress. Int J Biol Macromol 2010;47:603-13.
21. Ghassemi P, Wang J, Melchiorri AJ, et al. Rapid prototyping of biomimetic vascular phantoms for hyperspectral reflectance imaging. J Biomed Opt 2015;20:121312.
22. Bryarly MD, Tran MH, Ali A, Fei B. Retina phantom model for hyperspectral imaging. Proc SPIE Int Soc Opt Eng 2025; 13408:1340824.
23. Alexander RG, Macknik SL, Martinez-Conde S. Microsaccade characteristics in neurological and ophthalmic disease. Front Neurol 2018;9:144.
24. Pan MK. Targeting the fundamentals for tremors: the frequency and amplitude coding in essential tremor. J Biomed Sci 2025;32:18.
25. Clark AM, Intoy J, Rucci M, Poletti M. Eye drift during fixation predicts visual acuity. Proc Natl Acad Sci U S A 2022; 119:e2200256119.
26. Kaluzny J, Li H, Liu W, et al. Bayer filter snapshot hyperspectral fundus camera for human retinal imaging. Curr Eye Res 2017;42:629–35.
27. Zhang J, Zhang Y, Qian M, Zhang X. Light consistency correction for the liquid crystal tunable filter hyperspectral imaging system. J Opt Soc Am A Opt Image Sci Vis 2024;41: 1089-97.
28. Tran MH, Bryarly M, Pruitt K, et al. A high-resolution hyperspectral imaging system for the retina. Proc SPIE Int Soc Opt Eng 2024;12836:1283604.
29. Delori FC, Webb RH, Sliney DH. American national standards institute. Maximum permissible exposures for ocular safety (ANSI 2000), with emphasis on ophthalmic devices. J Opt Soc Am A Opt Image Sci Vis 2007;24:1250-65.
30. Zhao J, Lan R, Tan H, et al. Detection and characterization of microplastics and nanoplastics in biological samples. Nat Rev Bioeng 2025;3:1019-33.
31. Nihart AJ, Garcia MA, El Hayek E, et al. Bioaccumulation of microplastics in decedent human brains. Nat Med 2025;31: 1114-9.
32. Salvia R, Cañaveras M, Rico LG, et al. Prospective investigation of nanoplastic accumulation in healthy subjects, autoimmune diseases, hematological malignancies, lung cancer, and murine models. Microplastics 2025;4:1.
33. Yong CQY, Valiyaveettil S, Tang BL. Toxicity of microplastics and nanoplastics in mammalian systems. Int J Environ Res Public Health 2020;17:1509.
34. Jurowski K, Noga M, Kobylarz D, et al. Multimodal imaging using Raman spectroscopy and FTIR in a single analytical instrument with a microscope (infrared Raman microscopy AIRsight, Shimadzu): opportunities and applications. Int J Mol Sci 2024;25:6884.
35. Hermabessiere L, Himber C, Boricaud B, et al. Optimization, performance, and application of a pyrolysis-GC/MS method for the identification of microplastics. Anal Bioanal Chem 2018;410:6663-76.
36. Shi B, Patel M, Yu D, et al. Automatic quantification and classification of microplastics in scanning electron micrographs via deep learning. Sci Total Environ 2022;825:153903.
37. Friebel M, Roggan A, Müller G, Meinke M. Determination of optical properties of human blood in the spectral range 250 to 1100 nm. J Biomed Opt 2006;11:034021.
38. Zonios G, Dimou A, Bassukas I, et al. Melanin absorption spectroscopy: new method for noninvasive skin investigation and melanoma detection. J Biomed Opt 2008;13:014017.
39. Mizushima M, Kawamura T, Takahashi K, Nitta K. In situ

near-infrared spectroscopic studies of the structural changes of polyethylene during melting. Polym J 2012;44:162-6.
40. Rasheed M, Moosad K, Nampoori PBV, Sathianandan K. Overtone spectra of styrene and polystyrene in the visible and near infrared regions. Pramana J Phys 1989;33:391-5.
41. Jackson RS, Wang Q, Lien J. Data preprocessing method for the analysis of spectral components in mixtures. Appl Spectrosc 2022;76:81-91.
42. Rinnan Å, van den Berg F, Engelsen SB. Review of standard normal variate and other preprocessing methods. TrAC Trends Anal Chem 2009;28:1201-22.
43. Campanale C, Massarelli C, Savino I, et al. A detailed review study on potential effects of microplastics and additives of concern on human health. Int J Environ Res Public Health 2020;17:1212.
44. Shoup DN, Smith AE, Schultz ZD. Reduction of spectral overlap in spectral surface-enhanced Raman spectroscopy imaging using a dove prism. Appl Spectrosc 2025;79:2825–40.
45. Brazma A, Hingamp P, Quackenbush J, et al. Minimum information about a microarray experiment (MIAME)-toward standards for microarray data. Nat Genet 2001;29:365-71.
46. Nelson G, Boehm U, Bagley S, et al. QUAREP-LiMi: a community-driven initiative to establish guidelines for quality assessment and reproducibility for instruments and images in light microscopy. J Microsc 2021;284:56-73.
47. Rodrigues EM, Hemmer E. Trends in hyperspectral imaging: from environmental and health sensing to structure-property and nano-bio interaction studies. Anal Bioanal Chem 2022; 414:4269-79.
48. El-Mahrouk M, Langner C, Sucher R, Kniepeiss D. Introducing hyperspectral imaging as a novel tool for assessing donor liver quality during machine perfusion: a case report. World J Transplant 2025;15:102798.
49. Studier-Fischer A, Bressan M, Qasim A, et al. Spectral characterization of intraoperative renal perfusion using hyperspectral imaging and artificial intelligence. Sci Rep 2024;14: 17262.
50. Moulla Y, Buchloh DC, Köhler H, et al. Hyperspectral imaging (HSI)-a new tool to estimate the perfusion of upper abdominal organs during pancreatoduodenectomy. Cancers 2021;13:2846.
51. Hu Q, Wang X, Jiang J, et al. Exploring the spectral prior for hyperspectral image super-resolution. IEEE Trans Image Process 2024;33:5260-72.

Online supplementary material:

Appendix A. Detailed phantom recipe.

Appendix B. Statistical power calculations for both ex vivo and in vivo pilot experiments.

Appendix C. Computational simulation protocol.

Appendix D. Computational simulation data.

Appendix E. Quantitative detection feasibility analysis.